

Global dynamical structures from infinitesimal data

Benjamin McInroe*

*University of Pennsylvania and
University of California, Berkeley*

Robert J. Full

University of California, Berkeley

Daniel E. Koditschek

University of Pennsylvania

Yuliy Baryshnikov

University of Illinois, Urbana-Champaign

(Dated: October 4, 2024)

Discovering mechanisms underlying the behaviors of complex, high dimensional, and nonlinear dynamical systems is a central goal of the natural and synthetic sciences. Breakthroughs in machine learning in concert with increasing capacities for computation and data collection have enabled the use of trajectory measurements for learning predictive models. However, rigorous approaches for interpreting mechanisms from such models remain elusive, and asymptotic prediction accuracy suffers if the model does not capture important state space structures (e.g., attracting invariant sets). These limitations are especially pressing for system-level behaviors such as whole-body locomotion, where discontinuous, transient, and multiscale phenomena are common and prior models are rare. To take the next step towards a theory and practice for dynamical inference of complex multiscale systems in biology and beyond, we introduce VERT, a framework for learning the attracting sets that characterize global system behavior without recourse to learning a global model. Our approach is based on an infinitesimal-local-global (ILG) framework for estimating the proximity of any sampled state to the attracting set, if one exists, with formal accuracy guarantees. We demonstrate our approach on phenomenological and physical oscillators with hierarchical and impulsive dynamics, finding sensitivity to both global and intermediate attractors composed in sequence and parallel. Application of VERT to human running kinematics data reveals insight into control modules that stabilize task-level dynamics, supporting a longstanding neuromechanical control hypothesis. The VERT framework thus enables rigorous inference of underlying dynamical structure even for systems where learning a global dynamics model is impractical or impossible.

Ever more ubiquitous computation and burgeoning data sets promise to reveal the mechanisms that underlie the behavior of complex dynamical systems directly from observation data. Data-driven modeling is particularly valuable for biological and complex engineered systems. Their macroscopic behaviors emerge from coupled, nonlinear, and closed-loop dynamical interactions between large numbers of degrees of freedom (DoFs), themselves carrying dynamics that typically span multiple spatiotemporal scales and levels of organization. However, the elucidation of mechanisms - in particular, the discovery of dynamic and control processes and subsystems that give rise to and stabilize task-level behavior - remains a significant challenge. Experimental limits to state observability and input excitations can present significant obstacles to dynamics learning methods whose underlying computational models may often impose inductive priors that reach beyond the scope of scientifically available hypotheses.

To take the next step towards a data-driven paradigm for hypothesis informed discovery in general complex

systems data, we introduce an *infinitesimal-local-global* (ILG) framework that uses only generic (linear, infinitesimal) models of the dynamics to infer the persistent attracting state space structures that guide the global asymptotic system behavior. As a concrete application setting of broad interest, we focus our presentation on prospects for elucidating dynamics and control principles underlying agile and energetic legged locomotion behaviors, where characteristically high dimensional, discontinuous (hybrid), and nonlinear dynamics present significant obstacles to standard modeling approaches [1]. However, the theory and algorithms we develop are general, assuming only necessary conditions for local structural stability of the attractor, and we thus expect broad applicability of our framework to data-driven analysis of complex systems.

Recent breakthroughs in applied machine learning have seen the development of sophisticated approaches that leverage measured trajectory data, conceived as the output of some hidden dynamical system, and using those observations to learn a model that minimizes a system-specific prediction error. Linear [2, 3] and nonlinear [4-7] dimensionality reduction can reveal latent variables that capture variance, but do not explicitly account for the

* Corresponding Author: bmcinroe@seas.upenn.edu

temporal structure of trajectory datasets that contains critical information about underlying dynamics. Both can fail to capture structure necessary for understanding control mechanisms [8]. Another paradigm conjectures that observed trajectories are the outputs of dynamical systems and uses trajectory observations to learn a model that minimizes a system-specific prediction error. Exemplar approaches employ a range of approximation classes including linear dynamic modes, sets of nonlinear basis functions, and neural networks, and show that impressive prediction accuracy can be achieved by formulating the learning problem using insight from methods including Koopman theory [9, 10], symbolic regression [11, 12], and sparse regularization [12]. Further modifications to the model fitting procedure can improve accuracy by incorporating inductive priors from dynamical systems theory. For example, the loss function used for model training can be modified to promote more parsimonious coordinate representations [13], or to improve model reduction in systems with multiple time scales when a full order model is available [14]. A recent foundational approach uses spectral submanifold theory to learn reduced models of nonlinear dynamics as extended normal forms, demonstrating significant improvements to prediction accuracy for mechanical oscillations [15]. However, if the observations are not well approximated by a known (or hypothesized) continuous dynamical system, the need to select a global approximation class and learning criteria *a priori* presents a significant obstacle to learning an interpretable model that faithfully reproduces underlying mechanisms. The limitations of global model identification can be reduced by temporal segmentation of the trajectories into windows that are well approximated by linear dynamical systems [16, 17], or spatial segmentation of the domain into local charts that are more amenable to approximations of the nonlinear dynamics [18]. However, transitions between dynamical modes can reflect important mechanisms such as changing of constraints or internal control processes rather than limitations of the modeling apparatus [19].

Leveraging insights from differential topology [20] applied to the structure of hyperbolic invariant manifolds [21], we introduce the Vielbein Recovery of Templates (VERT) framework, an infinitesimal-local-global (ILG) paradigm for localizing persistent attracting submanifolds in output (observation) coordinates (Fig. 1). The infinitesimal component manifests itself in the assumption on the jets of the underlying dynamics, stipulating a decomposition of the tangent space into (integrable) distributions of contracting and neutral subspaces, which can be inferred from local data. The local existence of the integral submanifolds is phenomenologically strengthened to the existence of the global low-dimensional attractors and attendant basins of attractions [22] [23]. This broad framework shares with much of the prior literature the widely held premise that dynamical behavior of physical interest is typically characterized by a collapse of dimension – the presence of a low-dimensional

attracting invariant submanifold onto which a system’s trajectories quickly converge within the nominally high dimensional physical state space.

Motivated by this insight, our central contribution is the development of a theory and computational procedure for isolating from observed trajectory data the global locus of the lower dimensional attracting submanifolds that carry the long term system behavior. Critically for biological applications, our approach achieves this analysis while circumventing the need to fit a global (or piecewise global) model of the vector field to the trajectory data. Specifically, we show that a ‘fiberwise distance estimator’ whose sublevel sets indicate trajectory segments on or close to an attracting set can be constructed from infinitesimal-scale, linear dynamics estimated from local samples in a pointwise manner, affording localization of these loci of characteristic behavior without prior commitment to any parameterized model or structural assumptions beyond normal hyperbolicity — a necessary condition for their persistence under perturbations. Using models of both continuous and hybrid dynamical systems, we demonstrate the efficacy of our approach for discovering structurally stable attracting submanifolds with a range of geometric and dynamical properties without recourse to any other prior assumptions about the nature of the full system or attractor. Finally, we illustrate the applicability of our framework to postural trajectory data from motion capture of human treadmill running whose future systematic pursuit promises to reveal insight into the neuromechanical control of the hybrid, nonlinear dynamics underlying sensorimotor behavior.

BACKGROUND

Robust Behavior and Hyperbolic Attractors

A common modeling assumption is that characteristic system behaviors lie on or near a lower dimensional, often nonlinear space of latent variables in the full observable state space. However, the presence of external disturbances and internal control processes can perturb the state away from the lower dimensional latent space. Robustness to such disturbances requires that the latent space is an *attracting invariant set*, i.e., perturbed trajectories return asymptotically. Motivated by applications to experimentally measured data, we assume that the attracting invariant sets are locally *structurally stable*, that is, persistent under noise and perturbation. Normal hyperbolicity is a sufficient condition for local structural stability; for modeling purposes, we assume that detectable attracting sets are normally hyperbolic invariant manifolds (NHIM) [21].

Dynamic locomotion [24] provides a tractable behavior for exploring principles underlying robust, multiscale dynamical systems. The target behaviors of locomoting systems, typically translation and rotation of the body,

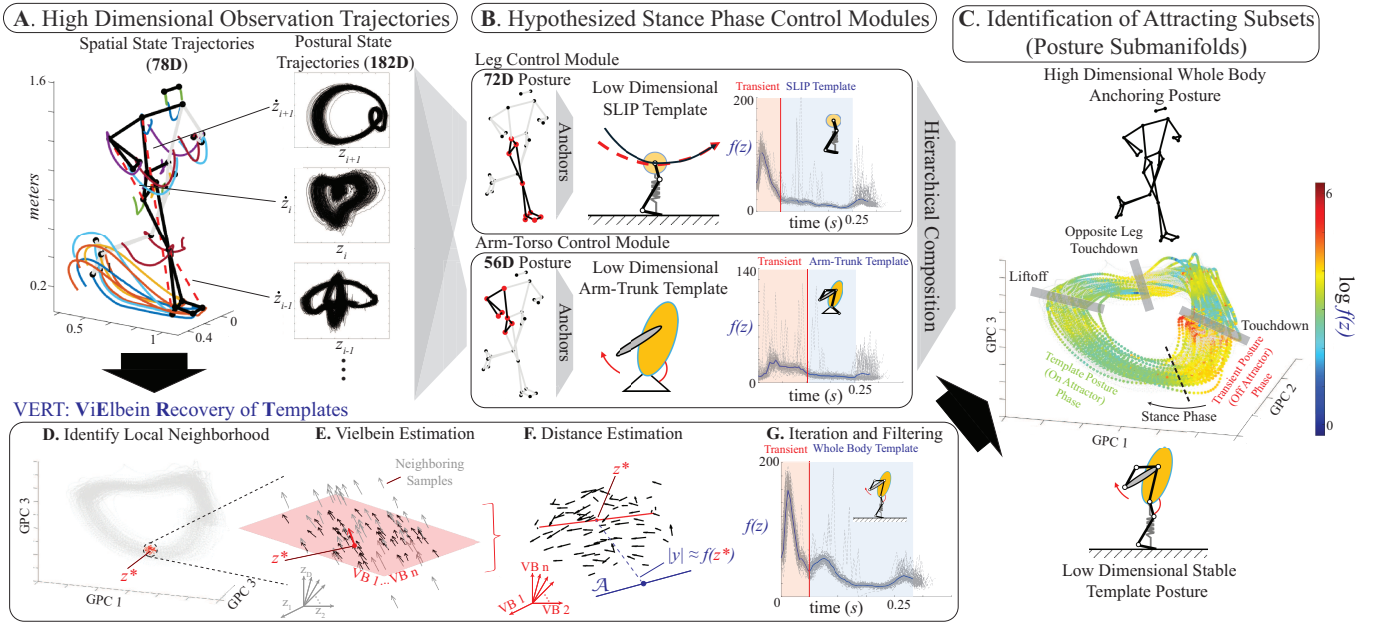


FIG. 1. Overview of the VERT computational framework. Panels (A–B) depict the relation to motivating hierarchical control hypotheses for complex, multi-scale systems, viewed through an illustrative application setting of the postural dynamics of human running. Panels (D–G) outline the steps of the VERT algorithm. **A.** Stable task-level system behaviors such as running emerge from the coupled, highly nonlinear, closed loop dynamics of many body segments and their interaction with the environment. **B.** We hypothesize that for many tasks, the global task-level behavior may be decomposed into hierarchically arranged control modules, whose coordinated interactions characterize the dynamics of appendages and body segments. The control module state spaces are embedded as submanifolds (postures) that carry the constituent dynamics (templates) of the full, coordinated system. **C.** We can use VERT to learn a spatiotemporal filter on the trajectory data that isolates locally stable (template) behavior from transient behaviors reflecting disturbances and stabilizing control (anchoring). **D.** VERT estimates the distance from each sample to the attractor guiding its asymptotic behavior ($f(z)$, Def. 1). The estimation procedure for a point z^* begins with identification of its metric nearest neighbors in state space. **E.** A Cartesian basis for the tangent space at z^* of the manifold containing the trajectories is estimated. The local subsample of the vector field (temporal differences, gray arrows) is projected onto the n -dimensional local vielbein basis (black arrows). **F.** Using this representation, we can estimate the component of the vector field on the vertical subspace, the local trivialization of the global, typically nonlinear vertical subbundle of the attractor. We can use this estimate to approximate the distance from z^* to its base point on the unknown attractor \mathcal{A} . **G.** Steps D–G are repeated for an appropriate number of samples. Filtering the trajectory data for sublevel sets of $f(z)$ reveals the posture carrying the template dynamics (blue) and hierarchical stabilization (anchoring) intervals of what subsequent hypothesis-informed analysis can posit as the stance leg and upper body posture during stance (See Fig. 5).

are both observable and interpretable. A longstanding question in the sensorimotor control of locomotion is how the abundance of muscles and joints in the body are coordinated to achieve a large and diverse set of typically lower dimensional tasks. The pioneering work of Nikolai Bernstein [25] suggests that whole body movements are constructed generatively from modular ‘submovements’. Modern electromyography (EMG) studies in both humans and non-human animals support the hypothesis that the neuromuscular system is organized into modular units (control modules) that can be recruited in series and parallel to accomplish high level motor tasks, and even recombined and fused through rehabilitative training when partial motor function is lost [26]. Advances in automated pose estimation provide the possibility of collecting large, rich kinematic trajectory datasets, affording the possibility of building surrogate data-driven models that reproduce these critical features of robust

sensorimotor behavior.

The templates and anchors framework (TAF) [1] articulates the control module hypothesis in the context of biomechanics and dynamical systems theory, stipulating that the characteristic postures of locomotion tasks lie on attracting invariant submanifolds (posture submanifolds) of the full postural state space. The posture submanifold and its restriction dynamics reveal the *template*, a low dimensional dynamical system that captures the target behavior for the task. This low dimensional system is *anchored* in the full (postural) state space by stabilizing control forces that render the posture submanifold attracting and invariant. Beyond the setting of locomotion, constructing a complex dynamical system from simpler subsystems is a ubiquitous approach for system synthesis and analysis [27]. In the following sections, we review the general setting of dynamical systems constructed from parallel or sequential composition of subsystems, with

motivating examples from dynamic locomotion and the TAF.

Parallel Composition of Attractors

In control module compositions from robotics, there is typically a great deal of choice in the geometry of the postures (the manner in which the template dynamics are embedded) and the relative strengths of the various anchoring gains that determine their relative time constants of attraction — and, thereby, the characteristic order in which trajectories approach the increasingly restricted succession of intersecting postures. Thus, from the viewpoint of robotics there is significant interest in not simply testing the TAF rendering of the control module composition hypothesis but in actually discovering what posture principles are associated with what kinds of compositions. This is the key question that our computational pipeline addresses.

To test the efficacy of our pipeline relative to this circle of ideas, we introduce a model of coupled Hopf-type oscillators anchored by a stable flow in a higher dimensional Euclidean space, the Anchored Hopf Model (A-HM). The structure of the coupled limit cycle modules of the A-HM is a first order phase oscillator, whose illustrated value is motivated by empirical and modeling studies of sprawled posture legged locomotion in insects [28], while the variously embedded postures (the coupled attracting invariant submanifolds) are motivated by the robotics examples [29–33]. Specifically, embedding of the coupled limit cycle system in the higher dimensional ‘posture’ space by a stabilizing vector field is motivated by a recent empirically validated algorithm for anchoring planar behaviors in spatial legged robots [33]. For our computational test system (Eqns. 1 & 2), the gains of the control forces that drive the state towards the limit cycle and entrain the two phase oscillators are set by the scalar parameters $\gamma_\rho > 0$ and $\gamma_\theta > 0$, respectively.

The template dynamics we consider within a Euclidean state space (with state $x \in \mathbb{R}^4$) is easiest to render in polar coordinates:

$$\begin{aligned}\dot{\rho}_i &= \gamma_\rho(1 - \rho_i)\rho_i \\ \dot{\theta}_i &= \omega + \gamma_\theta \sin(\theta_i - \theta_j)\end{aligned}\quad (1)$$

where $i, j \in \{1, 2\}$. Observe that the dynamics of the phase variables decouples from the amplitudes ρ , and has the structure of the Kuramoto oscillator system. The system entrains to a global limit cycle so long as $\gamma_\theta > 0$.

The reduced state space in which the limit cycles are anchored is in turn anchored in \mathbb{R}^D . For modeling purposes, we assume that the dynamics of the remaining coordinates is globally asymptotically stable e.g., is given by

$$\dot{y} = Ay \quad (2)$$

with a Hurwitz A , and $y = (y_5, \dots, y_D)$ is the vector of the auxiliary variables. The state vector for the full

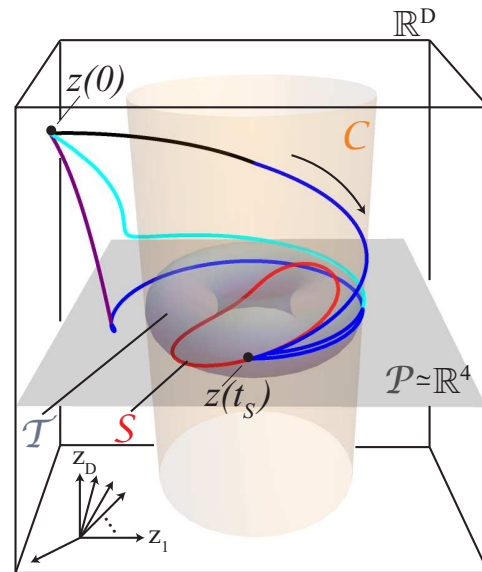


FIG. 2. Visualization of parallel anchoring hypotheses for the A-HM system described by Eqs. 1 & 2, with $\gamma_\theta \gg 0$. From the initial state $z(0)$, each trajectory approaches the limit cycle \mathcal{S} (red) asymptotically, represented here by $z(t_S)$. The relative values of control parameters ($\gamma_\rho, \gamma_\delta$) set the sequence of hierarchically arranged intermediate attractors that determine the behavior of the pre-limit cycle trajectory. Following Table I: \mathbf{H}_0 in red, \mathbf{H}_1 in cyan, \mathbf{H}_2 in purple, and \mathbf{H}_3 in black. Trajectory segments on their respective intermediate attractors are highlighted in blue (*c.f.*, Table I, Column 2).

system composed of Eqs. 1 & 2 is thus $(z_1, \dots, z_D) = (x_1, \dots, x_4, y_5, \dots, y_D) \in \mathbb{R}^D$. The rate of convergence to the anchored plane at $y = 0$ is set by the real part of the eigenvalues σ of A , $\Re\sigma = -\gamma_\delta$.

The behaviors realized by particular trajectories of the total system are determined by the relative magnitudes of the forces imparted by the control modules, the initial state, and the nature of perturbations to which the system is subjected, as in Fig. 2. The total system contains a hierarchy of attracting submanifolds whose appearance is governed by the relative strength of the gain parameters summarized in Table I that we now discuss. The lowest level of the hierarchy, towards which all initial conditions converge asymptotically, is a Hopf limit cycle, in the coupled case $\gamma_\theta > 0$. (If the oscillators are decoupled, i.e., if $\gamma_\theta = 0$, then the lowest dimensional attracting submanifold is the torus formed as the product space of the independent limit cycles.

This limit torus is anchored in the 4D subspace of the Hopf systems by the subsystems in Eq. 2, if the spectrum of A lies in the half-plane of $\{\Re\sigma < -\gamma_\rho\}$. If this is not the case, the state may converge to an annular subdomain of \mathbb{R}^D before reaching the 4D Hopf subspace, providing multiple qualitatively distinct routes for anchoring the lowest level template in the full system.

Subsystem Gain	Anchoring Hierarchy Hypothesis	VERT Detection Hypothesis
$(\mathbf{H}_0) \gamma_\theta \gg 0$	$z_i \in \mathbb{R}^d \rightarrow \mathcal{S} \ni z_f$	Detect \mathcal{S}
$(\mathbf{H}_1) \gamma_\rho \approx \gamma_\delta$	$z_i \in \mathbb{R}^d \rightarrow \mathcal{T} \rightarrow \mathcal{S} \ni z_f$	Detect \mathcal{T}
$(\mathbf{H}_2) \gamma_\rho \ll \gamma_\delta$	$z_i \in \mathbb{R}^d \rightarrow \mathcal{P} \rightarrow \mathcal{T} \rightarrow \mathcal{S} \ni z_f$	Detect $\mathcal{P}, \neg\mathcal{C}$
$(\mathbf{H}_3) \gamma_\rho \gg \gamma_\delta$	$z_i \in \mathbb{R}^d \rightarrow \mathcal{C} \rightarrow \mathcal{T} \rightarrow \mathcal{S} \ni z_f$	Detect $\mathcal{C}, \neg\mathcal{P}$

TABLE I. Table of hypothesized anchoring mechanisms (\mathbf{H}_{0-3}) for the Hopf system. We hypothesize the sequence of hierarchically embedded submanifolds that typical trajectories approach for each system configuration, and the expected behavior of the VERT pipeline if the hierarchy is detected.

Sequential Composition of Attractors

Analogous to the composition of control modules in state space described in the previous section, changes in target behavior or environment often necessitate the sequential composition of control modules in time. Achieving goal states while avoiding obstacles by back-chaining basins of attraction around successively targeted attractors by either design choice [34] or as necessitated by limited control affordance [35] represents a common instance of such nonsmooth, event-driven switches between stable continuous dynamics in the engineering control literature. However, even steady state locomotion behaviors, e.g., running with legs, involve impulsive changes in dynamics over the course of a single period as limbs make and break contact with the substrate. Each transition incurs the possibility of disturbances and postural errors that must be stabilized either by passive dynamics or active feedback control. The theory of hybrid dynamical systems provides a rigorous framework for the analysis and control of a broad array of such physically common systems that are parsimoniously modeled by imposing nonsmooth resets guarded by event-driven switches between distinct, smooth dynamical regimes [36, 37].

Relaxation oscillators offer a parametrically graded family of limit cycles that facilitate the study of nonlinear dynamics as they approach and begin to exhibit hybrid dynamical behavior [38]. In such systems, trajectories on the attracting limit cycle alternate between slow convergence along the cycle towards a near-equilibrium condition (relaxation) and fast, impulsive switches in the position of the equilibrium [38]. The van der Pol system is a canonical example of a relaxation oscillator when its bifurcation parameter that quantifies the strength of nonlinear damping exceeds a threshold. The alternation between slow, locally hyperbolic attracting dynamics and impulsive switches in the location of the local attractor provide an interpretable and relatively simple model in which to explore the anchoring of sequentially composed templates.

We use the anchored van der Pol (A-vdP) system, the cross product vector field of second order vector fields corresponding to the van der Pol system and an overdamped harmonic oscillator, as a testing example. In

Cartesian coordinates:

$$\begin{aligned}
 \dot{x}_1 &= x_2 \\
 \dot{x}_2 &= -\sin(x_1) + \mu(\cos^2(x_1) - 0.5)x_2 \\
 \dot{x}_3 &= x_4 \\
 \dot{x}_4 &= -x_3 - bx_4
 \end{aligned} \tag{3}$$

where the plane with coordinates (x_1, x_2) contains the van der Pol limit cycle, and (\dot{x}_3, \dot{x}_4) defines a (decoupled) vector field on (x_3, x_4) that anchors the limit cycle in \mathbb{R}^4 when the linear damping term b is positive. When the nonlinear damping μ is sufficiently large, the system exhibits relaxation oscillations.

VERT: VIELBEIN RECOVERY OF TEMPLATES

We introduce the Vielbein Recovery of Templates (VERT) framework, an ILG approach for identifying hierarchically embedded attracting sets from trajectory data. VERT takes a set of observed trajectories and returns the proximity of each point to the normally attracting invariant manifold (NAIM) that governs its asymptotic behavior. To establish a theoretical foundation for the computational heuristics used by VERT, we model the trajectories $\{z_i(t), t \in [0, T_i]\}_{i=1}^N$ as samples from the (possibly noisy) flow of a dynamical system (\mathcal{M}, ξ) , where \mathcal{M} is a piecewise smooth Riemannian manifold of dimension n , and $v : \mathcal{M} \rightarrow T\mathcal{M}$ is a piecewise $C^{r \geq 1}$ vector field. We assume the trajectories are embedded in a Euclidean observation space \mathbb{R}^D .

In the data-driven regime, we have access only to discretely sampled trajectories, and lack the coordinate representations of the tangent and normal bundles typically necessary to estimate their restriction dynamics. We thus employ insights and heuristics from the theory of normally hyperbolic invariant manifolds. Our approach is to define a *distance estimator* (Def. 1) that evaluates proximity of a sampled state to the attracting set in the *fiberwise* sense. We proceed by establishing modeling assumptions necessary to analyse the behavior of the fiberwise distance estimator.

Let $\mathcal{A} \subset \mathcal{M}$ be an invariant submanifold of dimension a for (\mathcal{M}, v) : $\phi_t(\mathcal{A}) \subset \mathcal{A}, t > 0$, for ϕ being the flow associated to the vector field v . We will denote by $U \supset \mathcal{A}$ a tubular neighborhood of this submanifold [20] which is attracted to \mathcal{A} . Normal Hyperbolicity implies that the trajectories starting in the neighborhood U converge to \mathcal{A} , exponentially fast, uniformly in some fixed Riemannian structure. We can introduce, locally, a privileged coordinate system $z = (x, y)$ on U , such that the coordinate x parameterizes the points of \mathcal{A} , while the attractor is given by $\mathcal{A} = \{y = 0\}$. The fibers \mathcal{F}_x of the projection $(x, y) \mapsto x$ are the analogues of the *stable manifolds* for the hyperbolic dynamics, trivialized through the selected coordinate system. We notice that

this coordinate system does not have to (and in fact, almost never does) extend to a global one. However, its usage provides a convenient modeling setting, and leads to the heuristic assumptions outlined below [39].

Fix a vicinity \mathcal{A}_U in the attractor, over which our coordinate system is defined, such that the tangent spaces to fibers at the points $(x, 0)$ are exponentially contracted. Now we will explicitly state our heuristic assumptions by expressing a version of normal hyperbolicity in local coordinates (x, y) . The vector field v describing the dynamics of the system can be represented, near a point $x_* \in \mathcal{A}_U$ as

$$v_x = \begin{pmatrix} u_0 + S(x, y) \\ A_1 y + T(x, y) \end{pmatrix} = \begin{pmatrix} u_0 \\ A_1 y \end{pmatrix} + B(x, y). \quad (4)$$

Here $u_0 = v(x_*, 0) \in T_{x_*} \mathcal{A}$ is the value of the vector field at $(x_*, 0) \in U$, and $S(x, y)$ captures the vanishing at $(x_*, 0)$ horizontal component of the vector field v . Similarly, $A_1 y + T(x, y)$ captures the split of the vertical component into the linear (in y) and non-linear parts. We remark that in the standard formalism of hyperbolic sets [40], the term S depends on x only, but we will not need this constraint. The mapping B describes the residual components of the vector field after the minimal approximations of (slow) motion along the attractor and exponential convergence towards it are extracted (nonlinearities, noise, cross-terms, etc). While we do not have direct access to these terms (as they depend on the coordinate system (x, y) , knowledge of which is equivalent to recovery of both the attractor and the stable foliation), this model of the infinitesimal behavior of the vector field can be used to establish a procedure to estimate the proximity of a point, $z_* = (x_*, y_*)$ to \mathcal{A} . Let $H := D_z v$ and $G := D_z B$ be the Jacobian matrices of mappings v and B , respectively.

Definition 1 *The fiberwise distance estimator is given by*

$$f(z) := |H(z)v(z)|$$

We note that the Jacobian H does not depend on the choice of the selected coordinate system, and that the determination of G relies on the local identification of the vicinity of z_* with a real linear space, but not on a specific splitting of the space into x and y factors. To understand the behaviour of the distance estimator f notice that in the ideal, linear setting, the local vector field is given by Eq. 4 with $B(y) = 0$. In this case, by inspection, the fiberwise distance estimator is equal to $|A_1^2 y_*|$, so that $\hat{f}(z_*)$ grows linearly with the distance from z_* to \mathcal{A} . Of course, the presence of noise and nonlinearities presents an obstacle to this reasoning. We proceed by showing that the behavior of $f(z_*) = f(x_*, y_*)$ with respect to $|y_*|$ can still be bounded so long as the residual component of the vector field is small relative to the hyperbolic component. We quantify this concept by introducing several constants, depending on the relative strength of the hyperbolic contraction.

Definition 2 *Let $C_G := \sup_{(x,y) \in U} \|G(x,y)\|$ be the upper bound on the operator norm of G . Further, consider the bounds on $C_+ := \sup_{x \in \mathcal{A}_U} \|A_1(x)\|$ the operator norms of A_1 and $C_- := \left(\sup_{x \in \mathcal{A}_U} \|A_1(x)^{-1}\| \right)^{-1}$ on the reciprocal of the operator norm of A_1^{-1} (so that $C_- |y| \leq |A_1(x)y| \leq C_+ |y|$ for $e \in \mathcal{A}_U$). Further, let $v_0 := \sup_{x \in \mathcal{A}_U} |v(x, 0)|$.*

Conceptually, C_G describes how strong the vector field v deviates from local linearity in y and constancy in x . The constant C_- expresses the strength of the contraction towards the attractor. Ideally, C_G is small and C_- is large. Note, however, that $C_- \leq C_+$.

Definition 3 *The error bound is given by*

$$E(\rho) = C_G((2C_+ + C_G)\rho + v_0)$$

Observe that the error bound grows quadratically with C_G .

Theorem 1 *In the notation of Definitions 1 and 3,*

$$C_-^2 |y| - E(|y|) \leq f(z) \leq C_+^2 |y| + E(|y|)$$

We provide a proof of Theorem 1 in Appendix I. The key implication of this result is that for sufficiently small C_G , the estimator f will be away from 0 together with the distance $|y_*|$ to the attractor, in a quantifiable manner, allowing one to ascertain the proximity to it. We remark that the definition, and therefore the estimation and computation of f , requires exclusively linear operations on local data in the neighborhood of a point, and does not depend on the split of the coordinate system into x and y , despite the fact that the formulation of our estimate does. By computing f for all (or an appropriate subsample) of the trajectory data, and then filtering the f -sublevel sets of the full trajectory dataset (geometrically, a *point cloud* in \mathbb{R}^D), we can isolate the set of trajectory segments that lie on or quantifiably near any physically relevant attractor \mathcal{A} in the *global* embedding (observation) space coordinates \mathbb{R}^D .

We detail algorithms for computing $f(z)$ on measurement data in the Supplement. The computation is, at a high level, performed as follows. First we estimate a local Cartesian basis for $T_{z_*} \mathcal{M} \simeq T_{x_*} \mathcal{A} \oplus \mathbb{R}^{n-a}$ and compute the restriction of the local vector field to this subspace v_{z_*} . Local PCA, performed on the subsample of points lying within an open Euclidean ball of radius r centered at z_* , provides a simple approach for computing a local basis of $T_{z_*} \mathcal{M}$ such that estimators for the tangent space and intrinsic dimension enjoy strong formal guarantees [41]. The local sample of the vector field $V_{z_*} : \mathbb{R}^D \rightarrow T \mathbb{R}^D$ can be approximated from finite differences. The local representation of the (n -dimensional) v_{z_*} can then be found by orthogonal projection of the (D -dimensional) V_{z_*} onto the vielbein basis. The Jacobian $H(z_*)$ can then be estimated by centering the local

vector field data and using linear estimation techniques; for experiments in the following sections, we use least squares regression with the standard MSE residual.

RESULTS

VERT is Sensitive to Attractor Hierarchies

Detecting the presence of subprocesses evolving on distinct time scales is critical for model inference and interpretation of systems constructed by parallel composition of stable subsystems. We hypothesize that the ILG nature of the VERT pipeline affords sensitivity to both the global and intermediate attracting sets through a detectable change in the behavior of the distance estimator along a trajectory as it transitions between them.

We test this hypothesis using simulated trajectories from the A-HM (Eqs. 1 & 2) while systematically varying the control parameters γ_ρ and γ_δ , which determine the timescale of convergence for the two subsystems. We use VERT to predict the trajectory segments that lie on the globally invariant attracting set, and then estimate the proximity of these segments to each intermediate attracting submanifold outlined in Fig. 2 using the MSE projection residual, with lower values indicating closer alignment with the hypothesized submanifold. For the submanifolds indicated in the rightmost column, the first column indicates the $(\gamma_\rho, \gamma_\delta)$ parameter regime where the projection residual should be minimal to support the hypothesis. The results are summarized in Fig. 3 for A-HM equations with and without a globally attracting limit cycle ($\gamma_\theta = 1$ and $\gamma_\theta = 0$, respectively).

Evaluation of the attracting set predictions from VERT (Fig 3C-D) support the hypothesis that the behavior of the distance estimator along typical trajectories reflects the locally dominant (i.e., fastest) component of the vector field. Visualizing the evolution of the distance estimator over a representative trajectory provides insight into how (Fig. 3A-B). We quantify the ground truth proximity of each point on the trajectory to the limit sets using the error coordinates e_ρ and e_δ , which are the Euclidean distances from the point to the surfaces $\{z : \rho_1, \rho_2 = 1\}$ and $\{z : y = 0\}$, respectively. Geometrically, e_ρ and e_δ are the Euclidean distances of the point to the attracting sets \mathcal{C} and \mathcal{P} in Table I, respectively. When γ_ρ is large relative to γ_δ and the initial state lies off of each subsystem's attracting set (quantified by the error coordinates, Fig. 3B), the rate at which the distance estimator converges initially outpaces the slower subsystem, reflecting the faster transient. After the fast transient has decayed (indicated temporally by the gray line \mathcal{C} in Fig. 3B and spatially by the gray 'cylindrical' point cloud in Fig. 3A), the behavior of the distance estimator rapidly switches, and converges at the rate of the slower system. Comparison of the results for systems with and without a limit cycle indicates an effect on the behavior of the distance estimator, with relatively higher

values of the projection residual persisting when $\gamma_\theta = 1$ and $\gamma_\delta > \gamma_\rho$. This is not unexpected - stabilizing the limit cycle effectively introduces a third time scale set by $|\gamma_\theta|$ - but does motivate further investigation of VERT for systems with more than two distinct time scales.

VERT Finds Continuous Attractors in Subdomains of Hybrid Systems

Detection of discontinuous or jump phenomena is necessary for inference of systems with non-smooth dynamics, such as legged locomotion or manipulation. The global dynamics of the A-vdP system are characterized by an attracting fixed point, Hamiltonian periodic orbits, or a limit cycle depending on the choice of damping parameters μ . We hypothesize that when μ is large and the global limit cycle exhibits relaxation oscillations, the ILG nature of VERT will afford sensitivity to not only the globally attracting limit cycle, but also to the local attracting dynamics *on* the limit cycle.

To test this hypothesis and explore the efficacy of VERT across dynamical regimes of the A-vdP system, we use VERT to predict attracting sets from simulated data for four values of the bifurcation parameter μ (Fig. 4). We compare representative predictions from VERT to the ground truth trajectories from the A-vdP system (Fig. 4B). The position coordinate of the anchoring subsystem, x_3 , goes to zero as the trajectory approaches the van der Pol subsystem plane. The acceleration of the van der Pol subsystem, \dot{x}_2 , only approaches zero asymptotically when the attracting set is a globally attracting fixed point ($\mu = -1$). Jump behaviors on the limit cycle are accompanied by a sudden change in the sign of \dot{x}_2 .

We visualize the spatial behavior of VERT predictions by projecting the trajectory data onto its first three GPCs (Fig. 4C). When $\mu = -1$, the locus of the attracting fixed point at the origin is apparent as the global minimum of $\log f(z)$. When the vector field in the van der Pol plane is Hamiltonian ($\mu = 0$), the distance estimator takes its minimum on the van der Pol plane, which is an attracting set for the anchoring subsystem. The periodic orbits have constant energy that increases with their radius; the behavior of the distance estimator is accordingly approximately constant over individual orbits, with this steady state value decreasing with orbit energy. When μ is positive and sufficiently large, the vector field in the van der Pol plane is much stronger than the anchoring vector field. The value of the distance estimator peaks sharply at the locus of jumps on the limit cycle, and is minimal when the trajectory is near the pair of locally attracting limit points on the slow phase of the limit cycle. While the limit cycle is globally attracting, the VERT predictions reveal the locally stable and unstable segments. It is worth noting that while superficially, VERT recovers only fragments of the (exponentially) stable limit cycle, this is enough to reconstruct all of it, given the global convergence properties.

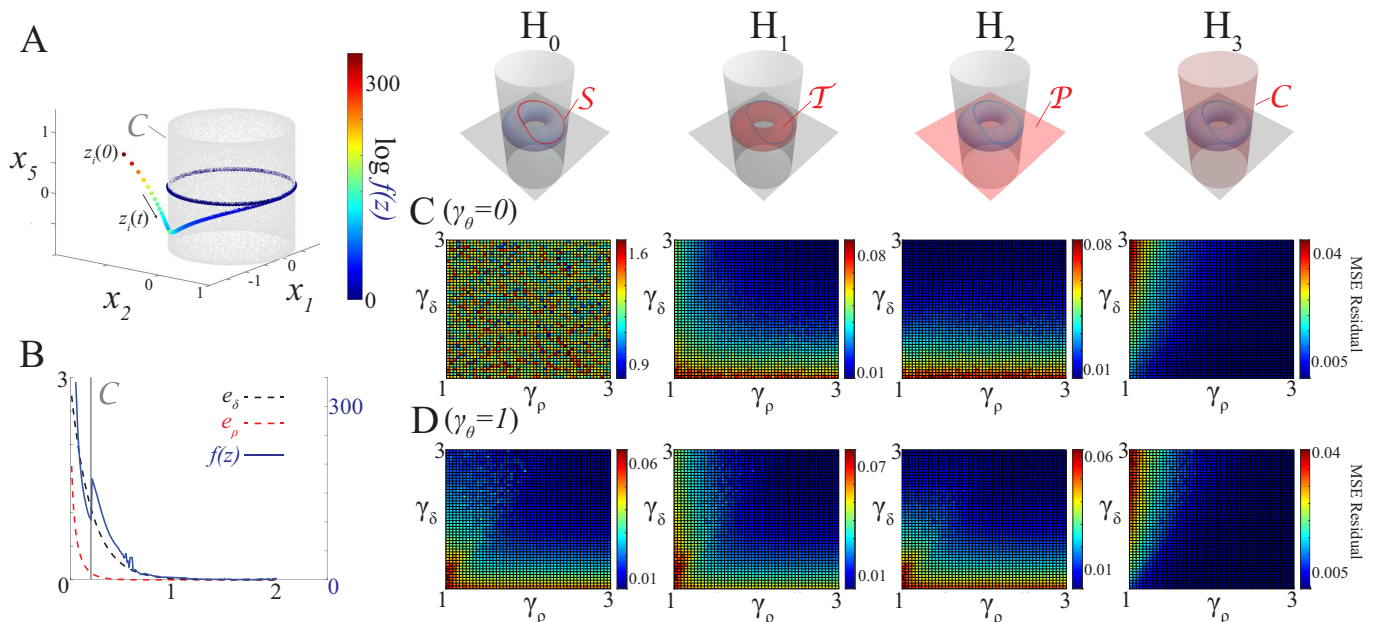


FIG. 3. VERT distance estimator is sensitive to attractor hierarchies. **A.** Visualization of a trajectory $z_i(t)$ for a system with control parameters $\gamma_\theta = 1$, $\gamma_\rho = 2$, $\gamma_\delta = 1$. From \mathbf{H}_3 (Table I), we expect the trajectory to first reach the submanifold \mathcal{C} (visualized in grey) before reaching the limit cycle \mathcal{S} . **B.** Representative plot of the distance estimator $f(z)$ (blue), and error coordinates for the intermediate attracting sets \mathcal{P} (e_δ , black dashed) and \mathcal{C} (e_ρ , red dashed). The grey line indicates when the trajectory reaches \mathcal{C} , corresponding to a local minimum of $f(z)$. After the γ_ρ control module has converged, the behavior of $f(z)$ is determined by the remaining γ_δ control module. The global minimum of $f(z)$ aligns with convergence to the attracting limit cycle \mathcal{S} at the lowest level of the attractor hierarchy. **C-D.** We sweep combinations of the parameters ($\gamma_\rho, \gamma_\delta$) to test sensitivity of $f(z)$ to intermediate attractors for systems without (**C.**, $\gamma_\theta = 0$) and with (**D.**, $\gamma_\theta = 1$) a limit cycle. Each column corresponds to an attracting submanifold hypothesis (c.f., Table I). The MSE residual captures relative proximity of the identified ‘template’ trajectory segments to the column’s submanifold, with lower values indicating closer proximity.

VERT Reveals Control Modules in Running Data

Predictions from the VERT framework benefit from trajectory datasets containing large variation in initial states and rich time-dependent disturbances, as samples on the fiber of the attracting set provide valuable data for estimating the vertical component of the linearized vector field. However, even relatively steady state legged locomotion behaviors contain considerable variability due in part to the presence of sensorimotor noise and latency. Postural kinematic variability is often excluded from behavior analysis during pre-processing, e.g., by projecting trajectories onto reduced latent coordinates such as global principal components to highlight stereotyped features that are useful for downstream tasks such as segmentation and labeling [43]. However, recent experimental and simulation studies on human running show that this intrinsic variability contains critical information for explaining task-level stability mechanisms [44]. Even in less energetic behaviors such as manual grasping, trajectory components excluded by both linear and nonlinear dimensionality reduction contain task-specific structure that could be valuable for understanding sensorimotor control [8].

We test the efficacy of VERT for discovering attracting

sets in real postural dynamics data using an open source dataset of whole-body human treadmill kinematics [45] (published in [46]). Bipedal running is an ideal setting for validating the performance of VERT, as interpretable and empirically validated template-anchor models such as the spring loaded inverted pendulum (SLIP) [42] and their characteristic kinematics can be readily extracted from the trajectories for comparison with the predictions from VERT. Because the SLIP template model represents a single virtual leg restricted to the sagittal plane, we focus our analysis on sensors from the right side of the body during the stance phase to facilitate comparison (Fig. 5A).

The VERT predictions for the whole body template are shown in Fig. 5B-C. Visualizing the distance estimator over the spatiotemporal projection of the trajectories onto their leading GPCs (Fig. 5B) reveals a phase of transient postural dynamics immediately following impact, with closest proximity to the template posture occurring during the latter half of stance. Temporal alignment of the distance estimator with the vertical ground reaction force (F_z) shows that the initial post-impact transient predicted by VERT aligns with the impact transient phase of F_z (Fig. 5C, red shaded region), and decays near the transition to the post-transient (SLIP-like) GRF profile. Interestingly, VERT predicts the persis-

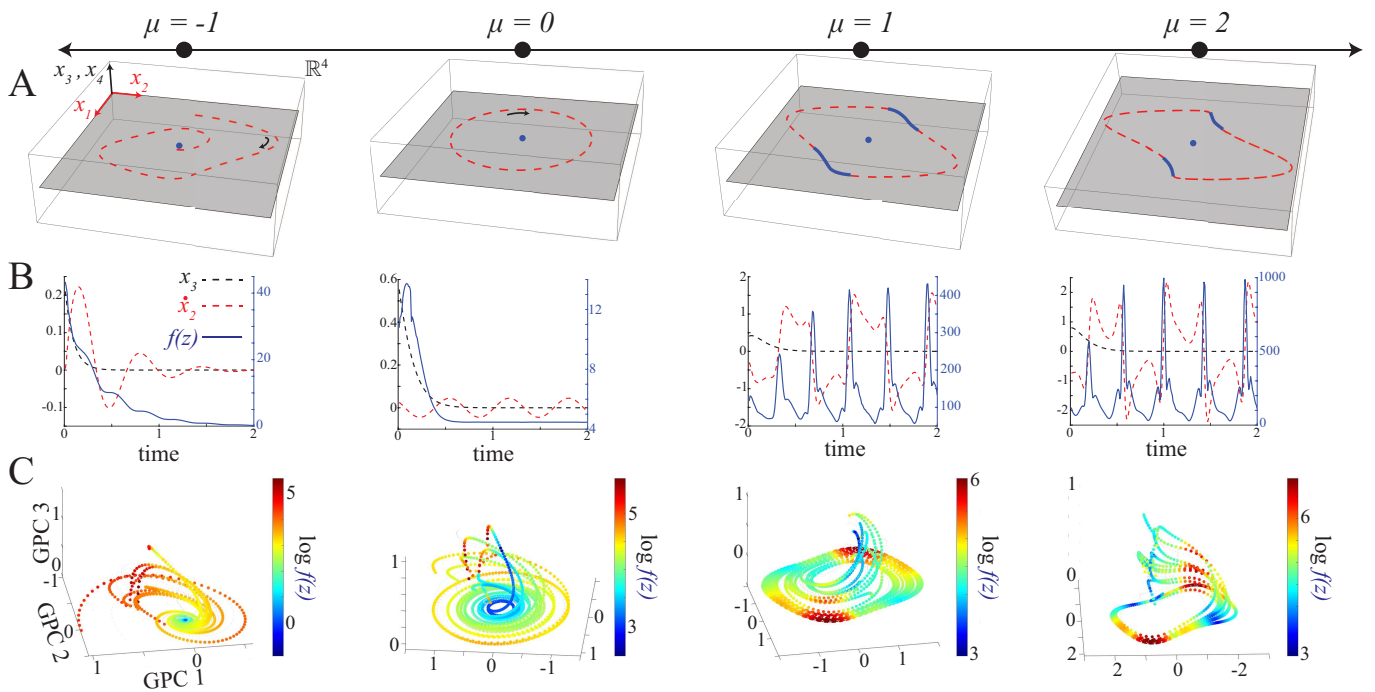


FIG. 4. VERT predicts locally stable regions across continuous and hybrid behaviors in the van der Pol system. **A.** Hierarchical and sequential attractors of Eq. 3 across the nonlinear damping parameter μ . The grey plane (x_1, x_2) contains the van der Pol vector field, and is globally attracting. Within the van der Pol plane, red curve segments depict highly impulsive regions along the attracting limit cycle while blue curve segments depict the more slowly evolving regions. **B.** Representative trajectory time series for the distance estimator $f(z)$ (blue), the position variable of the anchoring system (\dot{x}_3, \dot{x}_4) (black dashed), and the acceleration of the van der Pol oscillator \ddot{x}_2 (red dashed). **C.** Visualizations of the trajectory datasets plotted with respect to their leading three global principal components (GPCs), and colored by magnitude of the distance estimator. Low values of the distance estimator indicate predict the locus of a locally hyperbolic attracting set. The highly impulsive episodes of the van der Pol oscillator disturb the predictions, which, otherwise, accurately locate the limit cycle locus, suggesting the distance estimator’s utility for detecting hybrid behavior.

tence of a weaker transient following the transition to SLIP-like GRF behavior. This transient decays near the functional transition from energy absorption to propulsion, where the slope of F_z changes sign.

These predictions support the longstanding practice of modeling running dynamics as a hybrid limit cycle system. The results of our experiments in the preceding sections suggest that we can take a step further towards identifying the responses of specific appendages and body segments (i.e., control modules) to impact by first projecting the trajectories to the corresponding subspace of the full observation space, and then applying VERT to infer convergence of the projected dynamics to the global attracting set. We explore two control module hypotheses informed by existing template-anchor models of running dynamics: a control module for the leg posture (Fig. 5D), and a control module for the arm and torso posture (Fig. 5E).

The SLIP template and its anchoring in more detailed leg morphologies [47] suggest that the stance leg targets the behavior of a virtual spring. However, empirical measurements of ground reaction forces and COM kinematics show SLIP-like behavior only after an initial transient

phase following impact. The distance estimator for the leg projection converges after the F_z impact transient (Fig. 5E), with the second transient apparent in the full body projection absent, supporting the hypothesis that the initial postural transient results from stabilization of the SLIP posture. We estimate the length of the ‘virtual leg’, l_v , as the distance from the COM to the right medial ankle marker. Note that only postural variables were used by VERT, so information about the COM position and l_v was not directly available to VERT when computing the distance estimator. Convergence of the distance estimator to its sublevel set coincides with the transition to SLIP-like kinematics for l_v , further supporting that VERT has accurately predicted the transition to the template posture.

Whole-body template models that include arm and trunk dynamics are relatively less studied, in part due to the difficulty of inferring the control target of the more complex multi-body mechanical system. The sublevel set, determined by inspection (Fig. 5D), coincides with the propulsive phase of stance (the phase following the peak of the vertical GRF). Interestingly, the template phase predicted by VERT coincides with the transition

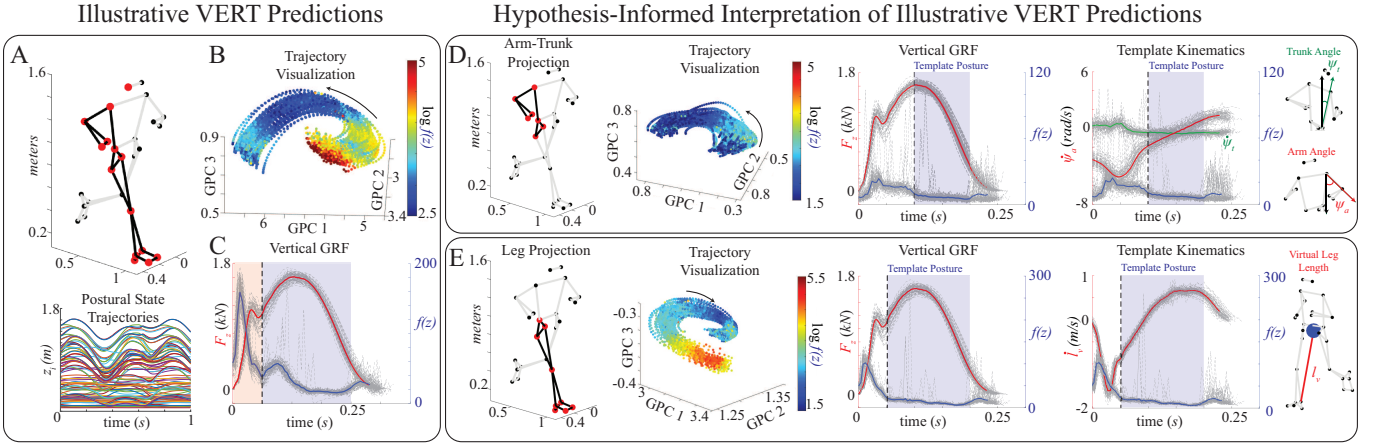


FIG. 5. Illustrative VERT predictions of running control modules are supported by comparison to empirically validated template models. **A.** The postural state data input to VERT are presented as trajectories through the space of spatial pairwise distances (and their velocities) between body markers, $z \in \mathbb{R}^{182}$. **B.** Visualization of the stance phase postural trajectories colored by value of the distance estimator, projected onto the first 3 global principal components (GPCs) of the postural state space. Arrow indicates direction of flow, from impact to lift-off. **C.** Stance phase averaged time series (with shadowed data traces) of the distance estimator $f(z)$, aligned with vertical ground reaction force (GRF) F_z . **D-E.** We use VERT to search for control modules in the Arm-Trunk (**D**) and Leg (**E**) postural state projections. We align and compare the averaged distance estimator $f(z)$ to the average vertical GRF time series (F_z) and kinematics informed by template hypotheses - the trunk and arm pitch angles (ψ_t and ψ_a , respectively, in row **D**) and the virtual leg length from the COM to heel (l_v in row **E**). The template phase of stance predicted by VERT aligns with the canonical kinematic behavior of the SLIP model [1, 42].

to nominally steady state kinematics of the arm posture, quantified by the spatial angle between the proximal segment of the stance arm and the gravity vector (ψ_a). The trunk-gravity pitch angle (ψ_t) also exhibits steady state behavior during the predicted template phase, although the onset occurs prior to the convergence of the distance estimator to the sublevel set, suggesting sensitivity primarily to the arm swing dynamics for the arm-trunk projection. Note that both ψ_a and ψ_t contain privileged information (orientation with respect to gravity) not used by VERT to compute the distance estimator. These results suggest that arm swing dynamics may have an important role for task-level control during the propulsive phase of stance, motivating further study.

DISCUSSION

We have proposed VERT, a framework for using observed trajectory data to estimate the attracting sets that govern their asymptotic behavior (Fig. 1). We show that the relative fiberwise proximity of a measured state to the locally strongest attracting set can be estimated using a model agnostic, infinitesimally (i.e., pointwise) motivated linear calculation, applied to only a spatially local subsample of the full dataset, enabling inference of the global qualitative behavior of the system without recourse to a particular global model of the dynamics. The VERT framework complements existing approaches for learning predictive dynamics models from data, which typically assume post-transient training data [14], by providing a

procedure to isolate transient trajectory segments from the full dataset. Because VERT does not require fitting a global model, this can be done in pre-processing. VERT further affords the ability to discover dynamical structure (the locus of attracting sets) from data that may be less amenable to global autoregressive model fitting due to the complexity of the underlying dynamics (e.g., presence of multiscale and discontinuous phenomena) and obstacles to model interpretation (e.g., systems that lack ground truth constitutive models). Stable attracting sets provide critical insight into the mechanisms underlying the dynamics of biological systems including locomotion [42], gene regulatory networks [48], and neural population dynamics [49]. We thus expect broad utility of VERT for learning models of biological and engineering systems, where the behavior of observed trajectories is strongly influenced by persistent disturbances and internal closed loop control processes.

We demonstrated the efficacy of VERT for accurately identifying attracting sets in synthetic data from dynamical systems with both parallel (Fig. 3) and sequential (Fig. 4) hierarchies, and experimentally measured human running kinematics (Fig. 5). Our results show that when subsystems with different characteristic time scales are simultaneously active, VERT estimates the distance to the attracting set of the locally dominant subsystem, affording sensitivity to and potentially inference of such parallel hierarchies. In systems with hybrid or jump-like behaviors, VERT detects the locally stable attracting sets on continuous subdomains of the global attracting set. In the human running data, which exhibits features of both parallel and sequential dynamical hierarchy, this

sensitivity suggests inference of potential control modules during the stance phase of running. The sublevel sets of the distance estimator accurately predict the phases of stance where ground truth kinematic observables exhibit template behavior, e.g., SLIP-like leg length dynamics and vertical GRF profile. Mounting experimental evidence suggests sensitivity of muscle spindle primary afferents to the rate of change of loading force as a mechanism for reflexive stabilization of postural perturbations [50]. The VERT predictions of post-transient template phases of stance are characterized by linear or constant accelerations of the ‘template’ kinematic variables for the respective arm-torso and leg control modules, suggesting that the transient behavior may result from reflexive stabilization following impact. These observations support the possibility of using VERT to accurately predict muscle activation dynamics from motion capture data, a prospect with potential breakthrough applications for biomechanics, robotics, and simulation of human dynamics. VERT can further be used in experimental design to develop perturbation assays that untangle the roles of different postural control modules for stabilizing locomotion tasks.

Integration of the VERT pipeline with tools for geometric and topological inference is a natural next step — discovered posture submanifolds likely (e.g., almost always in robotics) have dimensions higher than 1, and are almost always highly nonlinear. This motivates developing a funnel to the computational pipes of Topological Data Analysis [51], allowing one to recognize, in a model-agnostic way, the topological structure of the underlying attracting set. As the attracting sets are still expected to be of relatively low dimensions, we conjecture that the available topological inferences (primarily, ranks of the homology groups) would be sufficient to achieve this goal. Once the underlying attracting set is recovered, the estimation of the template behavior — the dynamics on the attractor — could be achieved by the standard approximation tools [52, 53]. The promising results from the A-HM and A-vdP models motivate further work on inferences for systems with multiscale behavior. We showed that applying VERT to hypothesis-informed projections of the human postural state can provide insight into the dynamics of particular appendages and body segments. Learning such projections directly from the outputs of VERT is an exciting prospect. To ensure our analysis of the human running data was refined to the stance phase, we used the independently measured vertical GRF signal to segment the full trial into phases when the right leg was in contact. In principle, integrating detection of hybrid reset events into VERT should be possible. The saltation matrix characterizes the first order variational update at a reset [54], and can be estimated from the local sample covariance matrices, which are already computed and stored by VERT to estimate the vielbein. Future work will explore the prospect of using such estimates to localize guard surfaces in state space.

MATERIALS AND METHODS

Hopf Dataset

Trajectories for the A-HM model were produced by integrating the model defined by Eqns. 1 & 2 using MATLAB’s ode45 function for the integration interval $[0 : 0.05 : 10]$. 10 polar coordinate pairs were sampled from the continuous uniform distributions $\rho \sim \mathcal{U}(2, 4)$ and $\theta \sim \mathcal{U}(0, 2\pi)$. For each polar coordinate pair (ρ, θ) , five initial conditions were computed by sampling: $(\rho, \theta) + \mathcal{N}(0, 0.3)$, producing a dataset of 50 trajectories. Trajectories were transformed to Cartesian coordinates before passing to VERT. To produce the plots in Fig. 3, control parameter combinations $(\gamma_\rho, \gamma_\delta)$ were produced from a uniformly spaced 50×50 grid with $\gamma_\rho, \gamma_\delta \in [1, 3]$. VERT was used to compute the distance estimator for 10 trajectories. The MSE residual was computed over these 10 trajectories. For each control parameter combination, we performed 5 trials each with independently sampled initial conditions, and the MSE residuals for each trial were averaged to produce Figs. 3C,D. Details for computing the MSE residuals are described in the Supplement. Code and parameters to reproduce the plots in Fig. 3 are available in the Supplement.

van der Pol Dataset

Trajectories for the A-VDP model were produced by integrating the model defined by Eqn. 3 using MATLAB’s ode45 function for the integration interval $[0 : 0.01 : 20]$. To produce the plots in Fig. 4, 20 initial conditions were independently sampled from the normal distributions: $x_1 \sim \mathcal{N}(0.5, 0.2)$, $x_2 \sim \mathcal{N}(0.3, 0.2)$, $x_3 \sim \mathcal{N}(0.5, 0.2)$, $x_4 \sim \mathcal{N}(0.1, 0.2)$. The numerical derivative \dot{x}_2 plotted in Fig. 4 was obtained using first order finite differences.

Human Running Data

The human running kinematics dataset consisted of a single continuous 4 min. trial (S3R1) obtained from the Dryad repository [45]. To parameterize the postural state of the right side of the body, we used the Euclidean distances between all pairwise combinations of the markers on the right side of the body as the position coordinates (see Supplement for marker labels), and the numerical derivatives of the position trajectories (obtained using finite differences) as the velocity coordinates, resulting in a state dimension of $2 \times \binom{14}{2} = 182$. The postural state trajectories were passed directly to the VERT pipeline. To produce the plots in Fig. 5, the vertical ground reaction force data was used to estimate right foot touchdown and liftoff events. The data was then aligned such that touchdown events occurred at $t = 0$ s. Mean trajectories for all variables over the stance phases were computed

by linearly resampling the data on a uniform interval and computing the means across trials at each time step. The projected datasets were obtained following the above procedure for the marker sets used in the upper and lower body projections.

ACKNOWLEDGMENTS

This work was funded in part by AFOSR HyDDRA MURI Award FA9550-23-1-0337 and in part by the University of Pennsylvania

I. APPENDIX

Proof of Theorem 1

We start with observing that $B(x_*, 0) = 0$, and that, by the standard bound via derivative,

$$|B(x, y)| = |B(x, y) - B(x_*, 0)| \leq C_G(|y| + |x - x_*|),$$

so that $|B(x_*, y_*)| \leq C_G|y_*|$.

Expanding the definition of the estimator $f(x_*, z_*) = |H(x_*, y_*)v(x_*, y_*)|$, we obtain (abbreviating $A_1(x_*)$ to A_1)

$$Hv = \left(\begin{pmatrix} 0 & 0 \\ 0 & A_1 \end{pmatrix} + G(x_*, y_*) \right) \left(\begin{pmatrix} u_0 \\ A_1 y_* \end{pmatrix} + B(x_*, y_*) \right).$$

Opening the brackets, we obtain the following sum:

$$\begin{aligned} & \begin{pmatrix} 0 \\ A_1^2 y_* \end{pmatrix} + \begin{pmatrix} 0 & 0 \\ 0 & A_1 \end{pmatrix} B(x_*, y_*) + G(x_*, y_*) \begin{pmatrix} u_0 \\ 0 \end{pmatrix} + \\ & G(x_*, y_*) \begin{pmatrix} 0 \\ A_1 y_* \end{pmatrix} + G(x_*, y_*) B(x_*, y_*). \end{aligned}$$

The norm of the second term is bounded by $C_+ C_G |y_*|$ (recall that $|B| \leq C_G |y_*|$); the norm of the third term is bounded by $C_G v_0$; of the fourth, $C_G C_+ |y_*|$, and of the fifth, $C_G^2 |y_*|$.

Further, as

$$C_-^2 |y_*| \leq |A_1^2 y_*| \leq C_+^2 |y_*|,$$

we obtain our result after a straightforward algebraic manipulation. \square

-
- [1] R. J. Full and D. E. Koditschek, Templates and anchors: neuromechanical hypotheses of legged locomotion on land, *Journal of experimental biology* **202**, 3325 (1999).
 - [2] G. J. Stephens, B. Johnson-Kerner, W. Bialek, and W. S. Ryu, Dimensionality and dynamics in the behavior of *C. elegans*, *PLoS computational biology* **4**, e1000028 (2008).
 - [3] M. T. Ciocarlie and P. K. Allen, Hand posture subspaces for dexterous robotic grasping, *The International Journal of Robotics Research* **28**, 851 (2009).
 - [4] G. J. Berman, D. M. Choi, W. Bialek, and J. W. Shaevitz, Mapping the stereotyped behaviour of freely moving fruit flies, *Journal of The Royal Society Interface* **11**, 20140672 (2014).
 - [5] L. Drnach, I. Essa, and L. H. Ting, Identifying gait phases from joint kinematics during walking with switched linear dynamical systems, in *2018 7th IEEE International Conference on Biomedical Robotics and Biomechanics (Biorob)* (IEEE, 2018) pp. 1181–1186.
 - [6] B. D. DeAngelis, J. A. Zavatone-Veth, and D. A. Clark, The manifold structure of limb coordination in walking *Drosophila*, *Elife* **8**, e46409 (2019).
 - [7] K. Luxem, P. Mocellin, F. Fuhrmann, J. Kürsch, S. R. Miller, J. J. Palop, S. Remy, and P. Bauer, Identifying behavioral structure from deep variational embeddings of animal motion, *Communications Biology* **5**, 1267 (2022).
 - [8] Y. Yan, J. M. Goodman, D. D. Moore, S. A. Solla, and S. J. Bensmaia, Unexpected complexity of everyday manual behaviors, *Nature communications* **11**, 3564 (2020).
 - [9] M. O. Williams, I. G. Kevrekidis, and C. W. Rowley, A data-driven approximation of the koopman operator: Extending dynamic mode decomposition, *Journal of Nonlinear Science* **25**, 1307 (2015).
 - [10] I. Mezić, Spectral properties of dynamical systems, model reduction and decompositions, *Nonlinear Dynamics* **41**, 309 (2005).
 - [11] M. Schmidt and H. Lipson, Distilling free-form natural laws from experimental data, *science* **324**, 81 (2009).
 - [12] S. L. Brunton, J. L. Proctor, and J. N. Kutz, Discovering governing equations from data by sparse identification of nonlinear dynamical systems, *Proceedings of the national academy of sciences* **113**, 3932 (2016).
 - [13] K. Champion, B. Lusch, J. N. Kutz, and S. L. Brunton, Data-driven discovery of coordinates and governing equations, *Proceedings of the National Academy of Sciences* **116**, 22445 (2019).
 - [14] S. E. Otto, G. R. Macchio, and C. W. Rowley, Learning nonlinear projections for reduced-order modeling of dynamical systems using constrained autoencoders, *Chaos: An Interdisciplinary Journal of Nonlinear Science* **33** (2023).
 - [15] M. Cenedese, J. Axås, B. Bäuerlein, K. Avila, and G. Haller, Data-driven modeling and prediction of nonlinearizable dynamics via spectral submanifolds, *Nature communications* **13**, 872 (2022).
 - [16] D. Del Vecchio, R. M. Murray, and P. Perona, Decomposition of human motion into dynamics-based primitives with application to drawing tasks, *Automatica* **39**, 2085 (2003).
 - [17] A. C. Costa, T. Ahamed, and G. J. Stephens, Adaptive, locally linear models of complex dynamics, *Proceedings of the National Academy of Sciences* **116**, 1501 (2019).
 - [18] D. Floryan and M. D. Graham, Data-driven discovery of intrinsic dynamics, *Nature Machine Intelligence* **4**, 1113 (2022).
 - [19] For example, the making and breaking of contact by ap-

- pendages during animal and robot locomotion induces transitions between characteristically nonlinear dynamical regimes, motivating the necessity of considering infinitesimal stability properties in determining where qualitative changes in behavior occur.
- [20] M. W. Hirsch, *Differential topology*, Vol. 33 (Springer Science & Business Media, 2012).
- [21] M. W. Hirsch, C. C. Pugh, M. Shub, and Hirsch, *Invariant Manifolds* (Springer, 1977).
- [22] J. Guckenheimer and P. Holmes, *Nonlinear oscillations, dynamical systems, and bifurcations of vector fields*, Vol. 42 (Springer Science & Business Media, 2013).
- [23] We remark that the VERT framework is applicable in hyperbolic dynamics where local contracting/expanding with respect to the offered Riemannian norm occurs only in some parts of the attractor (they need to occur *somewhere*, however, to satisfy the global hyperbolicity assumptions [55]). Once detected there, the normal hyperbolicity in broader regions can be inferred by extension along the trajectories. As an example, we cite van der Pol oscillators (whose entire limit sets satisfy the global criteria for hyperbolicity of [21], but lose a local attraction property in the standard Riemannian norm in the regions where the energy is pumped into the system by the “Coriolis term”).
- [24] M. H. Dickinson, C. T. Farley, R. J. Full, M. Koehl, R. Kram, and S. Lehman, How animals move: an integrative view, *science* **288**, 100 (2000).
- [25] N. Bernstein, *The coordination and regulation of movements* (Pergamon Press, 1967).
- [26] L. H. Ting, H. J. Chiel, R. D. Trumbower, J. L. Allen, J. L. McKay, M. E. Hackney, and T. M. Kesar, Neuro-mechanical principles underlying movement modularity and their implications for rehabilitation, *Neuron* **86**, 38 (2015).
- [27] A. MacFarlane, Information, knowledge and control, in *Essays on Control: Perspectives in the Theory and its Applications* (Springer, 1993) pp. 1–28.
- [28] S. Revzen and J. M. Guckenheimer, Estimating the phase of synchronized oscillators, *Physical Review E* **78**, 051907 (2008).
- [29] M. H. Raibert, *Legged robots that balance* (MIT press, 1986).
- [30] A. De and D. E. Koditschek, Parallel composition of templates for tail-energized planar hopping, in *2015 IEEE International Conference on Robotics and Automation (ICRA)* (IEEE, 2015) pp. 4562–4569.
- [31] A. De and D. E. Koditschek, Vertical hopper compositions for preflexive and feedback-stabilized quadrupedal bounding, pacing, pronking, and trotting, *The International Journal of Robotics Research* **37**, 743 (2018).
- [32] T. T. Topping, V. Vasilopoulos, A. De, and D. E. Koditschek, Composition of templates for transitional pedipulation behaviors, in *Robotics Research: The 19th International Symposium ISRR* (Springer, 2022) pp. 626–641.
- [33] T. Greco and D. E. Koditschek, Anchoring sagittal plane templates in a spatial quadruped, in *2023 IEEE International Conference on Robotics and Automation (ICRA)* (IEEE, 2023) pp. 12113–12119.
- [34] T. Lozano-Perez, M. T. Mason, and R. H. Taylor, Automatic synthesis of fine-motion strategies for robots, *The International Journal of Robotics Research* **3**, 3 (1984).
- [35] M. D. Kvalheim and D. E. Koditschek, Necessary conditions for feedback stabilization and safety, arXiv preprint arXiv:2106.00215 (2021).
- [36] A. J. Van Der Schaft and H. Schumacher, *An introduction to hybrid dynamical systems*, Vol. 251 (springer, 2007).
- [37] R. Goebel, R. G. Sanfelice, and A. R. Teel, Hybrid dynamical systems, *IEEE control systems magazine* **29**, 28 (2009).
- [38] A. A. Andronov, A. A. Vitt, and S. E. Khaikin, *Theory of Oscillators: Adiwes International Series in Physics*, Vol. 4 (Elsevier, 2013).
- [39] We use the German term *Vielbein* for frame, a local coordinate system to avoid contamination with the video processing context: the term is used in this meaning in the physics literature [56].
- [40] S. Smale, Differentiable dynamical systems, *Bulletin of the American mathematical Society* **73**, 747 (1967).
- [41] U. Lim, H. Oberhauser, and V. Nanda, Tangent space and dimension estimation with the wasserstein distance, arXiv preprint arXiv:2110.06357 (2021).
- [42] P. Holmes, R. J. Full, D. Koditschek, and J. Guckenheimer, The dynamics of legged locomotion: Models, analyses, and challenges, *SIAM review* **48**, 207 (2006).
- [43] A. E. Brown and B. De Bivort, Ethology as a physical science, *Nature Physics* **14**, 653 (2018).
- [44] N. Seethapathi and M. Srinivasan, Step-to-step variations in human running reveal how humans run without falling, *Elife* **8**, e38371 (2019).
- [45] H. Maus, S. Revzen, J. Guckenheimer, C. Ludwig, J. Reger, and A. Seyfarth, Data from: constructing predictive models of human running, *Dryad Digital Repository* (2014).
- [46] H.-M. Maus, S. Revzen, J. Guckenheimer, C. Ludwig, J. Reger, and A. Seyfarth, Constructing predictive models of human running, *Journal of The Royal Society Interface* **12**, 20140899 (2015).
- [47] U. Saranlı, W. J. Schwind, and D. E. Koditschek, Toward the control of a multi-jointed, monopod runner, in *Proceedings. 1998 IEEE International Conference on Robotics and Automation (Cat. No. 98CH36146)*, Vol. 3 (IEEE, 1998) pp. 2676–2682.
- [48] D. A. Rand, A. Raju, M. Sáez, F. Corson, and E. D. Siggia, Geometry of gene regulatory dynamics, *Proceedings of the National Academy of Sciences* **118**, e2109729118 (2021).
- [49] S. Vyas, M. D. Golub, D. Sussillo, and K. V. Shenoy, Computation through neural population dynamics, *Annual review of neuroscience* **43**, 249 (2020).
- [50] D. C. Lin, C. P. McGowan, K. P. Blum, and L. H. Ting, Yank: the time derivative of force is an important biomechanical variable in sensorimotor systems, *Journal of experimental biology* **222**, jeb180414 (2019).
- [51] J.-D. Boissonnat, F. Chazal, and M. Yvinec, *Geometric and topological inference*, Vol. 57 (Cambridge University Press, 2018).
- [52] W.-X. Wang, Y.-C. Lai, and C. Grebogi, Data based identification and prediction of nonlinear and complex dynamical systems, *Physics Reports* **644**, 1 (2016).
- [53] R. Yu and R. Wang, Learning dynamical systems from data: An introduction to physics-guided deep learning, *Proceedings of the National Academy of Sciences* **121**, e2311808121 (2024).
- [54] N. J. Kong, J. J. Payne, J. Zhu, and A. M. Johnson, Saltation matrices: The essential tool for linearizing hybrid dynamical systems, *Proceedings of the IEEE* (2024).

- [55] S. Smale, Differentiable dynamical systems, Bulletin (New Series) of the American Mathematical Society **73**, 747–817 (1967).
- [56] M. Nakahara, *Geometry, topology and physics* (CRC press, 2018).